Effects of Neoclassical Tearing Modes and Toroidal Field Ripple on Lost Alpha Power in the SPARC Tokamak

A E Braun
Plasma and Fusion Undergraduate Research Opportunities Intern

G J Kramer
Princeton Plasma Physics Laboratory, Princeton, NJ, USA

R A Tinguely
Plasma Science and Fusion Center, MIT, Cambridge, MA, USA

S D Scott
Commonwealth Fusion Systems, Cambridge, MA, USA

R M Sweeney
Plasma Science and Fusion Center, MIT, Cambridge, MA, USA

Abstract. Using the SPIRAL Monte Carlo, full particle-orbit simulation code [Kramer *PPCF* 2013], we investigate the effects of neoclassical tearing modes (NTMs) and toroidal field (TF) ripple on alpha power losses during steady-state operation of the SPARC primary reference discharge [Creely *JPP* 2020, Rodriguez-Fernandez *JPP* 2020]. Model perturbations for TF ripple and the $m/n = 2/1$ and $3/2$ NTMs with exaggerated widths selected based on an H-mode plasma approaching thermal quench are added to a simulated SPARC magnetic equilibrium through which marker particles are tracked. The $3/2$ and $2/1$ NTMs are located at $\rho_{pol} \sim 0.76$ and $\rho_{pol} \sim 0.86$ respectively, well positioned to increase alpha particle transport into and within an outer *lossy* region of the plasma beyond $\rho_{pol} \sim 0.8$ where over 95% of lost alpha particles are born [Scott *JPP* 2020]. Total alpha power losses are shown to increase modestly from 1.73% lost at a minimum to 2.34% lost at a maximum, and alpha particle surface power densities form localized hotspots on the first-wall near the low-field side midplane due to NTMs and TF ripple. We establish a conservative upper limit for first-wall alpha surface power densities on a toroidally symmetric wall for typical, flattop operation and motivate the consideration of NTMs in the design of three dimensional limiter surfaces for SPARC.

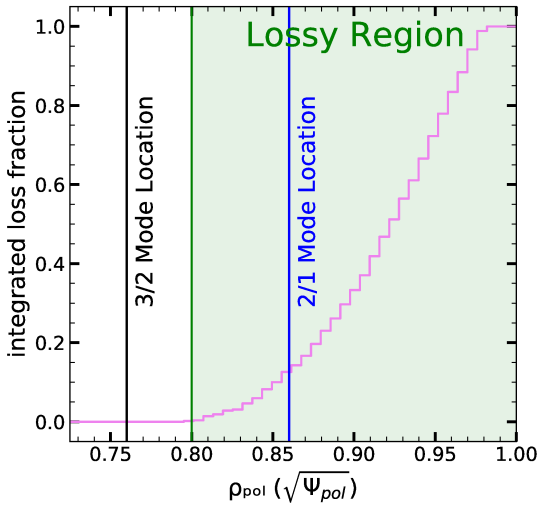

Figure 1: In violet, the integrated power loss fraction is shown as a function of ρ_{pol} , the square root of normalized poloidal flux, for 18 perfectly aligned TF coils without adding NTMs. The lossy region and the $m/n = 3/2$ and $m/n = 2/1$ mode locations are overlaid.

1. Introduction

SPARC is a compact, high-field tokamak currently being designed with a goal of reaching a fusion gain of $Q > 2$ but is projected to reach as high as $Q \approx 11$[1]. This prediction is based on simulations and analyses of the SPARC primary reference discharge (PRD)[2]. It is an H-mode discharge designed to have similar plasma dimensions to DIII-D with a major radius of 1.85 m and a minor radius of 0.57 m, but high-temperature superconducting magnets produce a magnetic field of 12.2 T on the magnetic axis which combined with a large plasma current of 8.7 MA leads to predictions of up to 140 MW of fusion power produced.

In deuterium-tritium (D-T) fusion, alpha power heating will exceed external heating when the plasma gain Q exceeds 5[3], so alpha power losses and surface power densities play a critical role in device performance expectations and first-wall power handling requirements. Previous simulations of SPARC investigated the effects of toroidal field (TF) ripple and found modestly increased alpha power losses and significantly higher first-wall surface power densities when including TF ripple[3]. In this paper, we study the effects of neoclassical tearing modes (NTMs) and their interactivity with TF ripple on alpha power losses in the SPARC tokamak.

NTMs'[4, 5, 6] deleterious effects on fast-ion confinement have been studied extensively since early theoretical predictions and experimental observations were made of appreciable fusion-born alpha particle losses due to low frequency MHD activity in TFTR[7, 8, 9]. Since then, in current, non-D-T tokamaks, research on the effects

of NTMs on fast-ions focused on losses of neutral beam (NB) non-inductive current drive[10, 11], broadening of NB parallel fast-ion current and fast-ion pressure profiles[12], and losses of suprathermal tail ions generated by ion cyclotron resonance heating and NBs[13, 14, 15]. For upcoming D-T tokamaks, similar research focuses on making predictions for alpha power losses. The effects of NTMs and TF ripple have been studied separately[16] and then together[17] in ITER resulting in increased peak heat loads in a loss pattern set by ripple effects. A similar study has also been performed for CFETR which in contrast to our results (sec. 3) found no synergistic effects between NTMs and TF ripple and also found no positive correlation between increasing NTM width and increasing alpha power losses[18]. While out the scope of this paper, extensive theoretical study has also been performed on the effects of NTMs[19, 8, 20, 14] and TF ripple[21, 22, 23] separately. To the authors' knowledge, analytic treatments have not been applied to the two effects combined.

In this paper, we study the most regularly observed NTMs, the 3/2 and 2/1 modes, which are located on the $q = 3/2$ surface at $\rho_{pol} \sim 0.76$ and on the $q = 2$ surface at $\rho_{pol} \sim 0.86$ respectively in the SPARC PRD[2] with q the magnetic safety factor and ρ_{pol} the square root of the normalized poloidal flux. As shown in fig. 1, the 3/2 mode is just outside and 2/1 mode is inside an outer "lossy" region of the plasma. This region beyond $\rho_{pol} \sim 0.8$ is the birth place of alpha particles accounting for over 95% of alpha power loss in the simulations performed in this paper and in ref. [3]. The modes are well positioned to increase alpha particle transport into and within this lossy region leading to increased alpha particle losses and surface power densities to the first wall. This investigation quantifies this effect in combination with the effects of TF ripple perturbations using the Monte Carlo, full-orbit following SPIRAL code[24] and shows large NTMs cause an intense focusing of alpha surface power densities on the first-wall near the low-field side midplane.

In section 2, we describe the use of SPIRAL to predict alpha power losses and surface power densities. We discuss the perturbations for TF ripple and NTMs which are added to a predicted SPARC PRD magnetic equilibrium. While it is unclear whether NTMs will be present in the SPARC PRD, we justify the selected NTM widths by imitating a plasma approaching a thermal quench in order to overpredict alpha power losses during typical, flattop operation consistent with H-mode operation.

In section 3, we discuss our simulation results showing increased alpha power losses up to 2.34% of the total alpha power due to NTMs and TF ripple. We show that there is synergy between TF ripple and NTMs causing significantly increased losses of alpha particles after multiple orbits, and that the effects resulting from combining multiple NTMs are less than additive considering total alpha power loss. Next, we discuss the increases in alpha particle heat loads and show that they are focused on the outboard first wall near the midplane. The practical consequences of these results are then discussed in section 4.

2. Simulation Setup

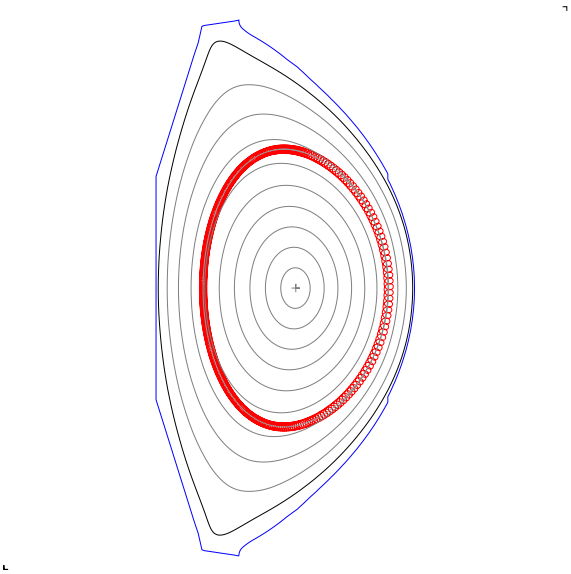

Figure 2: Diagram showing the simplified walls of SPARC used in SPIRAL in blue, last closed flux surface in black, equidistant normalized minor radii (square root of the normalized toroidal flux) in gray, and in red, an example of a 3.5 MeV alpha particle orbit, launched at $R = 1.8$ m and $Z = 0.6$ m with a pitch angle of 45° in the co-going direction, without considering electron drag or pitch angle scattering.

In order to calculate alpha power losses and first wall surface power densities, the Monte Carlo, full-orbit following SPIRAL code (SVN Version 144 of April 2021) tracks ensembles of alpha particle markers in a simulated SPARC PRD magnetic equilibrium perturbed by NTMs and TF ripple. In this section, we first address test particle tracking and selection of ensemble sizes. Then we explain the implementation of the magnetic equilibrium and NTM and TF ripple perturbations. Lastly, we justify the studied NTM widths and mode frequencies.

To begin the calculation of predicted alpha power losses and surface power densities, SPIRAL spawns ensembles of 3.5 MeV alpha particle markers uniformly distributed in volume and pitch angle. It then solves the Lorentz force equation for each of the markers and follows their paths accounting for interactions with the thermal plasma via a Lorentz scattering operator. This results in slowing-down and pitch angle scattering[24]. The particles are followed until they either collide with the wall and are marked as lost or are thermalized, due to collisional energy loss, at 1.5 times the local ion temperature after about 100 ms.

The test particles are then weighted to recover the SPARC PRD alpha birth profile as predicted by TRANSP [25] in the run discussed in ref. [2] assuming an equilibrium producing 22 MW of alpha power out of 112 MW of fusion power. From there the lost

alpha power and heat loads are calculated using a toroidally symmetric SPARC wall with simplified divertor shapes as shown in fig. 2. For calculating heat loads, the wall is divided into a grid of about 4000 tiles, each roughly 170 cm^2 in size, and impinging test particles' weighted power is summed.

For total alpha power loss studies, ensembles of 11,000 marker particles are used. The ensemble size is then increased to 51,000 marker particles to calculate first-wall heat loads in order to ensure statistically relevant heat load distributions.

The equilibrium magnetic field used for tracking the marker particles is calculated using the Tokamak Simulation Code [26] in the run discussed in ref. [1] while NTMs and TF ripple are added as perturbations. As outlined in ref. [24], care was to taken to ensure all magnetic fields are continuous and divergence-free.

The TF ripple magnetic perturbation is calculated using the Biot-Savart Law and added to the equilibrium[24]. Three ripple cases are considered in this study: no ripple, planned ripple, and upper-bound ripple. The no ripple case assumes an infinite number of TF coils resulting in a toroidally symmetric plasma. The planned ripple case assumes 18 perfectly mounted TF coils in accordance with the precise design of SPARC. The computed ripple contours for this configuration can be found in figure 1 in ref. [3]. In the upper-bound ripple case, the TF coils are given small displacements to account for possible coil misalignment during construction. The coils are displaced in and out according to a normal distribution with a standard deviation of 6 mm and a maximum of 9 mm. This serves as a worst case scenario for the TF ripple magnitude as the coils are expected to be mounted more accurately than the aforementioned tolerances. A plot of the toroidal field ripple magnitude as a function of major radius for in and out displaced coils can be found in figure 3 of ref. [3].

The NTMs are also implemented as a perturbation to the equilibrium magnetic field. An analytical model for the NTMs was used for the parallel component of the vector potential, $A_\parallel$, parameterized as:

$$A_\parallel = a_0 \Psi_N (1 - \Psi_N) e^{-[(\Psi_N - \Psi_0)/w]^2} e^{i(m\theta - n\phi - \omega t)} \tag{1}$$

with Ψ_N the normalized equilibrium poloidal flux, m and n the poloidal and toroidal mode numbers, θ and ϕ the poloidal and toroidal angles, and ω the mode frequency in the laboratory frame. The amplitude, a_0, was adjusted using a well established relation between the NTM amplitude and width[27] while the mode width, w, choice is discussed below. The mode location, Ψ_0, is adjusted so that the mode peaks at the resonant surface where $q(\Psi_0) = m/n$.

This investigation focuses on the 2/1 and 3/2 NTMs which are both regularly observed in tokamak plasmas. The 3/2 mode has been shown to reduce normalized volume-averaged plasma pressure by up to 20% in ASDEX Upgrade[28], and the growth of the 2/1 mode is often the precursor to NTM-induced thermal quenches[29]. The 2/1 and 3/2 NTMs are also of particular interest due to their respective locations inside and directly outside the outer lossy region as was shown in fig. 1.

NTM widths are challenging to predict due to their dependence on the classical

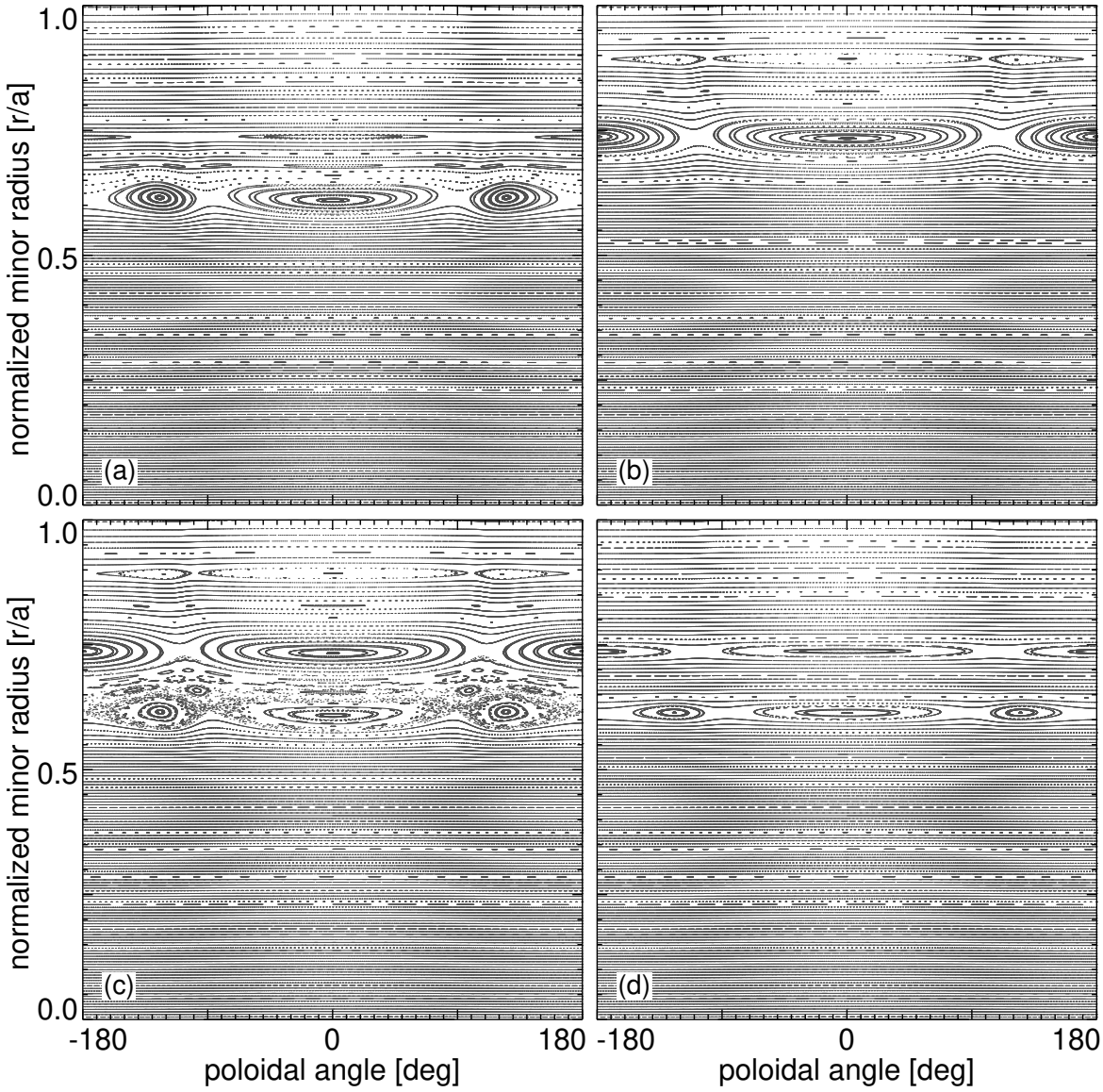

Figure 3: Poincaré Plots for relevant NTM cases: (a) Large 3/2 Mode ($w = 0.08$ in units of Ψ_N,$\sim$ 3 cm), (b) Large 2/1 Mode ($w = 0.12$ in units of Ψ_N,$\sim$ 6 cm), (c) Large Combined Modes (2/1 and 3/2), (d) Small Combined Modes (2/1 and 3/2, $w = 0.04$ in units of Ψ_N,$\sim$ 2 cm).

stability index[30] which is not well known for SPARC. Small values for the classical stability index lead to NTM decay or the formation of small, benign islands, and high values allow for larger NTM widths which couple with other NTMs and error fields eventually leading to 2/1 mode locking and a thermal quench[29].

In this study, we select NTM widths that indicate a likely inevitable thermal quench in order to provide an overprediction of losses for typical, flattop operation. We approximate a probable thermal quench scenario by choosing 3/2 and 2/1 mode widths which display stochastic fields around the 3/2 mode and non-stochastic fields around

the 2/1 mode as shown in fig. 3(c). Modest further increases in mode width result in the stochastization of fields around both modes which we take to indicate a thermal quench. Therefore this *large combined modes case* (fig. 3(c)) serves as an exaggerated NTM width case yet absent of major degradation to the plasma. Furthermore, we also studied a *small combined mods case* (figure 3(d)) and the large NTMs individually (figures 3 (a) and (b)).

For the majority of NTM cases, the phase of every island and the mode rotation frequencies are set to zero. The phases of the islands are set to zero, because large width NTMs' O-points align with the outboard midplane as they approach mode locking and thermal quench [29]. The mode rotation frequency is also set to zero such that localized surface power density hotspots display maximal heat loads and appear clearly. However, in rotating plasmas the mode frequency reflects the Doppler-shifted plasma rotation at the rational surface where the mode is localized. When toroidal rotation is set at 5.2 kHz and 6.5 kHz for the 2/1 and 3/2 modes respectively, consistently with the information provided in reference [31], the hotspots are distributed more evenly toroidally reducing the maximal heat loads. The effects of both rotating and non-rotating NTMs on first-wall surface power density distributions will be discussed further in the next section.

3. Results

In this section, we present and compare the increases in alpha power losses and surface power densities due to selected NTM and TF ripple cases. Table 1 displays the total percentage of alpha power lost for five NTM cases with the three ripple configurations. Similar to previous results[3], there is a clear trend of increased losses due to increasing magnitudes of TF ripple. Any addition of NTMs also increases the total losses at a maximum of 0.21% of the total alpha power or 46 kW in each ripple case when the large combined modes are added. The increase due to the small combined modes of 0.01% is minimal.

	Ripple Cases		
NTM Cases	None	Planned	Upper-bound
No Modes	1.73%	1.95%	2.13%
Small Combined	1.74%	1.95%	2.14%
Large 3/2	1.78%	2.01%	2.21%
Large 2/1	1.90%	2.12%	2.28%
Large Combined	1.91%	2.15%	2.34%
Difference between Large Combined and No Modes Cases	0.18%	0.20%	0.21%

Table 1: Percentage of total alpha power lost for each of the NTM and TF ripple cases, and an additional row showing the difference between the large combined modes and no modes cases for each ripple case.

Differences from No Modes Case

	Ripple Case		
NTM Cases	None	Planned	Upper-bound
Lg. 3/2 Mode	0.05%	0.06%	0.08%
Lg. 2/1 Mode	0.17%	0.17%	0.15%
Lg. Comb. Modes	0.18%	0.20%	0.21%
Sum of Individual Mode Differences	0.22%	0.23%	0.23%

Table 2: Calculations to justify the non-additive and non-synergistic effects of the 2/1 and 3/2 modes in percentage alpha power lost.

	Ripple Cases		
NTM Cases	None	Planned	Upper-bound
No Modes	34 kW	75 kW	116 kW
Small Combined	35 kW	78 kW	117 kW
Large 3/2	47 kW	90 kW	133 kW
Large 2/1	62 kW	110 kW	146 kW
Large Combined	63 kW	117 kW	160 kW

Table 3: Calculated non-prompt alpha power losses (kW) for each NTM and TF ripple case. In every case, the prompt alpha power losses are ~ 360 kW.

Furthermore, the 2/1 mode plays a more dominant role than the 3/2 mode in increasing alpha power losses. The losses due to the large 2/1 mode case are more comparable to the large combined modes case than the large 3/2 mode case which suggests that the 2/1 mode is responsible for a greater portion of the increased losses. This is likely due the location of the 2/1 mode within the lossy region as compared to the location of the 3/2 mode within the region of high confinement as shown in fig. 1.

Surprisingly, as shown in table 2, the effects of the large 2/1 and 3/2 modes are non-additive and non-synergistic. The effect of each mode case is taken to be the difference in total alpha power lost from the no modes case. The individual mode cases' effects are summed to show that they are greater than the large combined mode cases' effects.

We can then divide total alpha power losses into two types: prompt and non-prompt losses. Prompt losses occur on a time scale shorter than the bounce orbit transit time (~ 15 microseconds) and are minimally affected by perturbations in the plasma. They account for ~ 365 kW or $\sim 1.5\%$ of total alpha power for all cases studied here. The non-prompt losses occur on longer time scales and are caused by perturbations of the particle orbits by pitch angle scattering, TF ripple, and/or NTMs. The non-prompt losses, shown in table 3, account for a smaller fraction of the total losses but dominate in enhancement due to TF ripple and NTMs.

Once again, the effects of the the 2/1 and 3/2 modes are less than additive, and

the opposite, *synergy*, is displayed for the large NTM cases and each TF ripple case. As an example in table 3, the difference between the upper-bound ripple, large combined modes case (row 6, column 4) and the control case (row 2, column 2) is 126 kW while the sum of the individually considered perturbation's differences (row 6, column 2 and row 2, column 4) to the control case is 111 kW. Therefore the combined effect is greater than the sum of the individual effects. These synergistic non-prompt losses are compelling, but due to the dominance of the prompt power losses they account for only a small increase in the total alpha power loss.

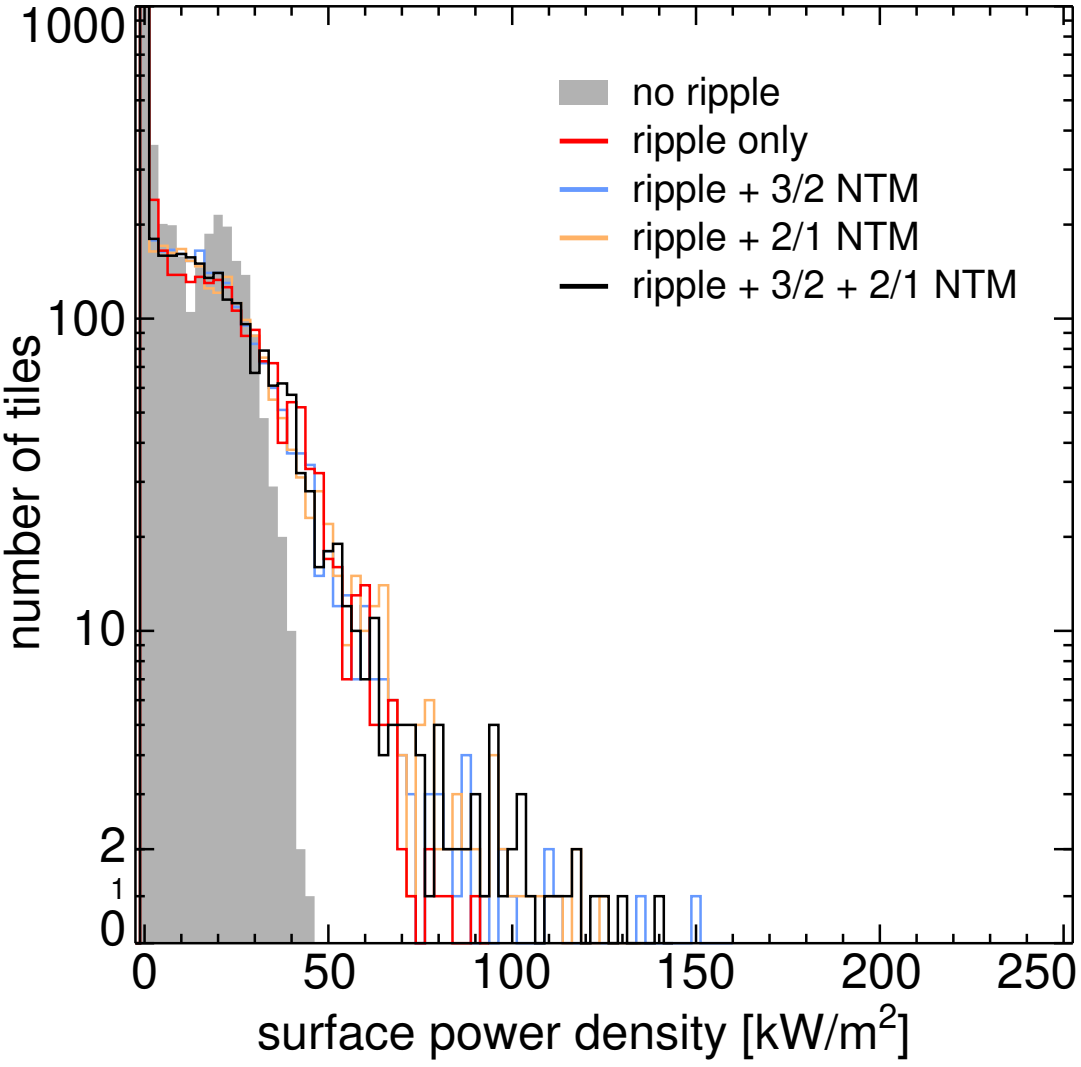

Figure 4: Toroidally symmetric wall power density occurrences are shown for a no ripple case and planned ripple cases for each NTM case. The scale transitions from linear to logarithmic at 2 tiles.

While prompt alpha particle losses are uniformly spread over the first wall above the midplane, non-prompt losses are localized at the low-field side midplane. Therefore, the enhanced non-prompt, first-wall alpha power losses appear as localized hotspots. Variation in the losses can be compared to a reference value of $\sim 20\,\mathrm{kW/m^2}$ assuming uniform spreading of the prompt losses above the midplane on a estimated wall geometry. Figure 4 displays heat load distributions based on ensembles of 51,000 marker particles and the toroidally symmetric grid discussed in sec. 2 for five cases: i) no ripple and no modes, ii) planned TF ripple only, iii) and iv) planned ripple with individual large width NTMs, and v) planned ripple with combined large width NTMs. Again similar to previous results [3], the inclusion of TF ripple significantly increases the maximum surface power density when compared to the no ripple case. Without TF ripple or NTM perturbations, the maximum first-wall surface power density is found to be less than $50\,\mathrm{kW/m^2}$ for this simplified wall geometry. Adding the planned TF ripple increases the maximum to about $90\,\mathrm{kW/m^2}$. The maximum is then further increased by the inclusion of the individual large width NTMs or the combined case up to about $150\mathrm{kW/m^2}$. While the precise maximum surface power density values for each NTM case are uncertain, the trend of distribution tails shifting towards higher heat loads is clear and indicates the formation of localized hotspots on a small number of wall tiles.

This hotspot appears near the midplane ($Z \sim -0.1$ m-0.4 m) as shown in a comparison between fig. 5(a), a planned ripple, no NTMs case and fig. 5(b), a planned ripple, large width combined NTM case. The toroidal symmetry of the losses is broken as the heat load is focused between about 90° and 150° in a single maximum pattern indicative of 2/1 mode dominance. The hotspot is then exacerbated by switching to an upper-bound ripple, large width combined NTM case in fig. 5(c).

This hotspot is responsible for the increased tails shown in fig. 4 but can be ameliorated by adding mode rotation. Fig. 5(d) is an upper-bound ripple case with large width, rotating, combined NTMs. In comparison to fig. 5(c), the localized hotspot of increased surface power density is spread roughly uniformly in the toroidal direction. Although not nearly as pronounced as the increased heat loads in the non-rotating, focused hotspot cases, the increases in losses near the midplane due to the NTMs is still present as shown in a comparison to fig. 5(a). In the next section, we discuss the implications of the modestly increased total alpha power losses and focused heat loads due to NTMs for SPARC operation and machine components.

4. Discussion and Conclusion

In this paper, alpha particle losses were studied in the presence of toroidal field (TF) ripple and the 3/2 and 2/1 neoclassical tearing modes NTMs for the SPARC tokamak. An ensemble of alpha particles was generated within a simulated SPARC PRD magnetic equilibrium perturbed by NTMs and TF ripple. These particles are then followed through their full gyro-orbits including electron and ion collisions until they either thermalize or are lost to a toroidally symmetric wall using the Monte Carlo SPIRAL

code.

It was found that in SPARC NTMs with exaggerated widths in combination with TF ripple increased the fusion-born alpha particle losses from 1.73% with no magnetic field perturbations to 2.13% including the worst case ripple scenario (upper-bound ripple) and to 2.34% when the worst case TF field ripple and largest combined NTM case were included (upper-bound ripple and large combined NTMs.) Increased losses of this magnitude are not expected to significantly detract from SPARC's performance and the goal of reaching a fusion gain of 2[1].

However, the localized increases in surface power densities could be concerning for SPARC PRD flattop operation. Radio frequency (RF) antennas are planned to be placed from the midplane to $Z \approx \pm 50$ cm[3]. The localization of increased surface power density due to the 2/1 NTM coincides with this band, so the 2/1 mode could damage the RF antennas, especially in a locked mode scenario. We calculate the increased, maximum surface power density in this location to be about $140\,\mathrm{kW/m^2}$ in the planned ripple, large combined mode case compared to only $90\,\mathrm{kW/m^2}$ in the planned ripple, no modes case using the toroidally symmetric SPARC wall. Numerical simulations show the tungsten first-wall tiles will begin approaching their recrystallization temperature due to a hotspot with a similar size and location to the one caused by the NTMs but with a surface power density increased to $\sim 5\,\mathrm{MW/m^2}$ in a 10-second SPARC plasma. The maximal first-wall surface power density computed here for a toroidally symmetric wall is well below that limit.

However, the three dimensional wall of SPARC includes recessed RF antennas and vertical limiters extending toward the plasma ~ 1 cm, which intentionally concentrate heat loads in order to protect the RF antennas. A future study will be performed to minimize the maximal surface power densities on limiter surfaces which will necessarily include NTMs' surface power density focusing.

The study should likely include full-orbit (FO) calculations of particle trajectories. A comparison between FO, hybrid FO and guiding-center (GC), and GC ASCOT simulations has been performed for ITER including TF ripple, test blanket modules, and ferric insert perturbations. It was found that FO following increases the average wall power load by a factor of about 3 and peak power load by a factor of about 5 when compared to pure GC calculations. It was also found that using a hybrid FO and GC scheme (in which GC is used while the particle is more than one Larmor radius away from the wall and FO is used within one Larmor radius) results in heat loads that fall in between the pure FO and GC simulations[32]. Therefore, it is likely important continue using FO simulations in order to study the upper limits of alpha surface power density.

Furthermore, other disagreements between our results and similar studies suggest the possibility of other NTM alpha particle loss dynamics not being captured within the GC formalism. Another study on the effect of only 2/1 and 3/2 NTMs in ITER using the ASCOT hybrid GC and FO particle tracking found that there is no redistribution of alpha power loads due to the inclusion of NTMs in contrast to our results[16]. Similarly in disagreement with our results, another study on alpha particle losses in CFETR due

to NTMs and TF ripple using GC particle tracking found that synergy between 2/1 and 3/2 NTMs and TF ripple was negligable and total losses were unaffected by NTM amplitude[18]. It is impossible to validate the conclusions of these papers and our own with experimental results as the tokamaks have yet to be built, but the data presented in this paper finds additional consequential effects of NTMs on alpha particle confinement. Therefore, we suggest further study on NTMs' effects on alpha particle losses to be carried out using FO particle tracking especially in devices with large Larmor radii compared to NTM widths as is the case for SPARC.

This study may also be extended to use NTM perturbations as calculated by NIMROD[33] or other 3D MHD codes. This would allow for more realistic perturbing fields from self-consistent calculations of the perturbation radial profile and relative NTM sizes. More core localized MHD activity such as sawteeth and Alfvén waves as well as edge localized perturbations such as error fields will also be studied in the future.

5. Acknowledgements

This work was made possible by funding from the Department of Energy for the Plasma and Fusion Undergraduate Research Opportunities (PFURO) program. This work is supported by the US DOE contract No. DE-AC02-09CH11466 and Commonwealth Fusion Systems. The United States Government retains a non-exclusive, paid-up, irrevocable, world-wide license to publish or reproduce the published form of this manuscript, or allow others to do so, for United States Government purposes.

References

[1] A. J. Creely, M. J. Greenwald, S. B. Ballinger, D. Brunner, J. Canik, J. Doody, T. Fülöp, D. T. Garnier, R. Granetz, T. K. Gray, and et al. Overview of the sparc tokamak. *Journal of Plasma Physics*, 86(5):865860502, 2020.

[2] P. Rodriguez-Fernandez, N. T. Howard, M. J. Greenwald, A. J. Creely, J. W. Hughes, J. C. Wright, C. Holland, Y. Lin, and F. Sciortino. Predictions of core plasma performance for the sparc tokamak. *Journal of Plasma Physics*, 86(5):865860503, 2020.

[3] S. D. Scott, G. J. Kramer, E. A. Tolman, A. Snicker, J. Varje, K. Särkimäki, J. C. Wright, and P. Rodriguez-Fernandez. Fast-ion physics in sparc. *Journal of Plasma Physics*, 86(5):865860508, 2020.

[4] P. H. Rutherford. Nonlinear growth of the tearing mode. *The Physics of Fluids*, 16(11):1903–1908, 1973.

[5] H. P. Furth, P. H. Rutherford, and H. Selberg. Tearing mode in the cylindrical tokamak. *The Physics of Fluids*, 16(7):1054–1063, 1973.

[6] Z. Chang, J. D. Callen, E. D. Fredrickson, R. V. Budny, C. C. Hegna, K. M. McGuire, M. C. Zarnstorff, and TFTR group. Observation of nonlinear neoclassical pressure-gradient–driven tearing modes in tftr. *Phys. Rev. Lett.*, 74:4663–4666, Jun 1995.

[7] S.J. Zweben, R.L. Boivin, M. Diesso, S. Hayes, H.W. Hendel, H. Park, and J.D. Strachan. Loss of alpha-like MeV fusion products from TFTR. *Nuclear Fusion*, 30(8):1551–1574, aug 1990.

[8] H. E. Mynick. Transport of energetic ions by low-n magnetic perturbations. *Physics of Fluids B: Plasma Physics*, 5(5):1471–1481, 1993.

[9] S.J Zweben, D.S Darrow, E.D Fredrickson, G Taylor, S. von Goeler, and R.B White. MHD induced alpha particle loss in TFTR. *Nuclear Fusion*, 39(9):1097–1109, sep 1999.

[10] C. B. Forest, J. R. Ferron, T. Gianakon, R. W. Harvey, W. W. Heidbrink, A. W. Hyatt, R. J. La Haye, M. Murakami, P. A. Politzer, and H. E. St. John. Reduction in neutral beam driven current in a tokamak by tearing modes. *Phys. Rev. Lett.*, 79:427–430, Jul 1997.

[11] E.M. Carolipio, W.W. Heidbrink, C.B. Forest, and R.B. White. Simulations of beam ion transport during tearing modes in the DIII-d tokamak. *Nuclear Fusion*, 42(7):853–862, jul 2002.

[12] K.E. Thome, X.D. Du, B.A. Grierson, G.J. Kramer, C.C. Petty, C. Holland, M. Knolker, G.R. McKee, J. McClenaghan, D.C. Pace, T.L. Rhodes, S.P. Smith, C. Sung, F. Turco, M.A. Van Zeeland, L. Zeng, and Y.B. Zhu. Response of thermal and fast-ion transport to beam ion population, rotation and t sube/sub/t subi/sub in the DIII-d steady state hybrid scenario. *Nuclear Fusion*, 61(3):036036, feb 2021.

[13] M García-Muñoz, P Martin, H.-U Fahrbach, M Gobbin, S Günter, M Maraschek, L Marrelli, H Zohm, and the ASDEX Upgrade Team. NTM induced fast ion losses in ASDEX upgrade. *Nuclear Fusion*, 47(7):L10–L15, jun 2007.

[14] Emanuele Poli, Manuel García-Muñoz, Hans-Ulrich Fahrbach, and Sibylle Günter. Observation and modeling of fast trapped ion losses due to neoclassical tearing modes. *Physics of Plasmas*, 15(3):032501, 2008.

[15] M. Gobbin, L. Marrelli, H.U. Fahrbach, M. Garcia-Muñoz, S. Günter, P. Martin, and R.B. White and. Numerical simulations of fast ion loss measurements induced by magnetic islands in the ASDEX upgrade tokamak. *Nuclear Fusion*, 49(9):095021, sep 2009.

[16] T. Kurki-Suonio, O. Asunta, E. Hirvijoki, T. Koskela, A. Snicker, T. Hauff, F. Jenko, E. Poli, and S. Sipilä. Fast ion power loads on ITER first wall structures in the presence of NTMs and microturbulence. *Nuclear Fusion*, 51(8):083041, jul 2011.

[17] A. Snicker, E. Hirvijoki, and T. Kurki-Suonio. Power loads to ITER first wall structures due to fusion alphas in a non-axisymmetric magnetic field including the presence of MHD modes. *Nuclear Fusion*, 53(9):093028, aug 2013.

[18] Baolong Hao, Roscoe White, Xiang Gao, Guoqiang Li, Wei Chen, Xiaojing Wang, Bin Wu, Muquan Wu, Xiang Zhu, Xiaodong Lin, Yinxian Jie, Qing Zang, Jiangang Li, and Yuanxi Wan. Numerical investigation of alpha particle confinement under the perturbation of neoclassical tearing modes and toroidal field ripple in cfetr. *Nuclear Fusion*, 61(4), 3 2021.

[19] R. B. White, R. J. Goldston, K. McGuire, Allen H. Boozer, D. A. Monticello, and W. Park. Theory of mode-induced beam particle loss in tokamaks. *The Physics of Fluids*, 26(10):2958–2965, 1983.

[20] H. E. Mynick. Stochastic transport of mev ions by low-n magnetic perturbations*. *Physics of Fluids B: Plasma Physics*, 5(7):2460–2467, 1993.

[21] R. J. Goldston and H. H. Towner. Effects of toroidal field ripple on suprathermal ions in tokamak plasmas. *Journal of Plasma Physics*, 26(2):283–307, 1981.

[22] R. J. Goldston, R. B. White, and A. H. Boozer. Confinement of high-energy trapped particles in tokamaks. *Phys. Rev. Lett.*, 47:647–649, Aug 1981.

[23] P.N. Yushmanov. Generalized ripple-banana transport in a tokamak. *Nuclear Fusion*, 23(12):1599–1612, dec 1983.

[24] G J Kramer, R V Budny, A Bortolon, E D Fredrickson, G Y Fu, W W Heidbrink, R Nazikian, E Valeo, and M A Van Zeeland. A description of the full-particle-orbit-following SPIRAL code for simulating fast-ion experiments in tokamaks. *Plasma Physics and Controlled Fusion*, 55(2):025013, jan 2013.

[25] R.V Budny, M.G Bell, A.C Janos, D.L Jassby, L.C Johnson, D.K Mansfield, D.C McCune, M.H Redi, J.F Schivell, G Taylor, T.B Terpstra, M.C Zarnstorff, and S.J Zweben. Simulations of alpha parameters in a TFTR DT supershot with high fusion power. *Nuclear Fusion*, 35(12):1497–1508, dec 1995.

[26] S.C. Jardin, J. Delucia, M. Okabayashi, N. Pomphrey, M. Reusch, S. Kaye, and H. Takahashi. Modelling of post-disruptive plasma loss in the princeton beta experiment. *Nuclear Fusion*,

27(4):569–578, apr 1987.

[27] Z. Chang, E. D. Fredrickson, S. H. Batha, M. G. Bell, R. V. Budny, F. M. Levinton, K. M. McGuire, G. Taylor, and M. C. Zarnstorff. Neoclassical tearing modes in tokamak fusion test reactor experiments. i. measurements of magnetic islands and . *Physics of Plasmas*, 5(4):1076–1084, 1998.

[28] S Günter, A Gude, M Maraschek, Q Yu, and the ASDEX Upgrade Team. Influence of neoclassical tearing modes on energy confinement. *Plasma Physics and Controlled Fusion*, 41(6):767–774, jan 1999.

[29] R. Sweeney, W. Choi, M. Austin, M. Brookman, V. Izzo, M. Knolker, R.J. La Haye, A. Leonard, E. Strait, and F.A. Volpe and. Relationship between locked modes and thermal quenches in DIII-d. *Nuclear Fusion*, 58(5):056022, mar 2018.

[30] R. Sweeney, A. J. Creely, J. Doody, T. Fülöp, D. T. Garnier, R. Granetz, M. Greenwald, L. Hesslow, J. Irby, V. A. Izzo, and et al. Mhd stability and disruptions in the sparc tokamak. *Journal of Plasma Physics*, 86(5):865860507, 2020.

[31] N. T. Howard, P. Rodriguez-Fernandez, C. Holland, J. E. Rice, M. Greenwald, J. Candy, and F. Sciortino. Gyrokinetic simulation of turbulence and transport in the sparc tokamak. *Physics of Plasmas*, 28(7):072502, 2021.

[32] A. Snicker, S. Sipilä, and T. Kurki-Suonio. Orbit-following fusion alpha wall load simulation for ITER scenario 4 including full orbit effects. *Nuclear Fusion*, 52(9):094011, sep 2012.

[33] C.R. Sovinec, A.H. Glasser, T.A. Gianakon, D.C. Barnes, R.A. Nebel, S.E. Kruger, S.J. Plimpton, A. Tarditi, M.S. Chu, and the NIMROD Team. Nonlinear magnetohydrodynamics with high-order finite elements. *J. Comp. Phys.*, 195:355, 2004.

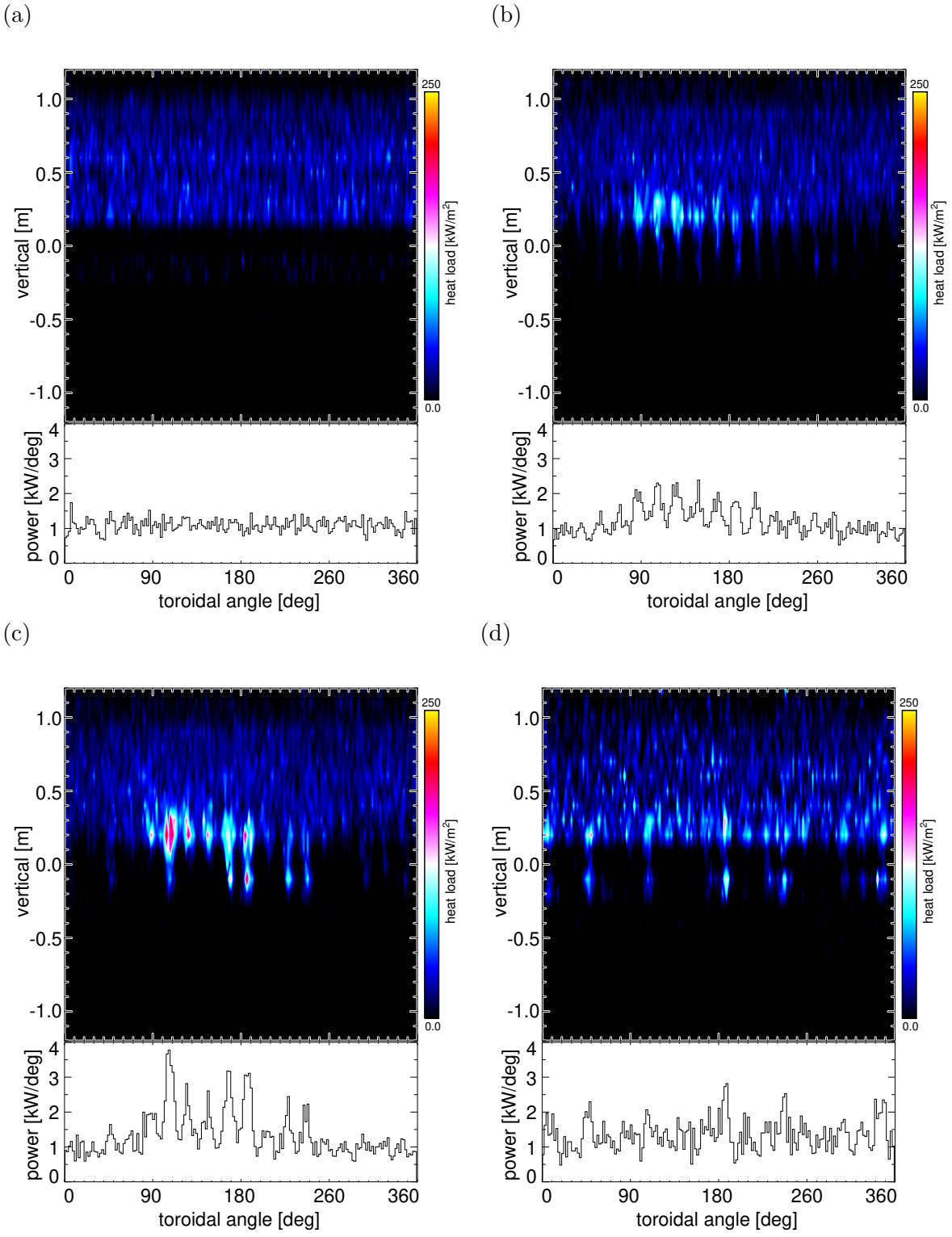

Figure 5: Surface power density maps for the outboard first wall for selected NTM and ripple cases: (a) No modes and planned ripple, (b) Large combined modes and planned ripple, (c) Large combined modes and upper-bound ripple, (d) Large combined modes rotating at the local plasma rotation frequency and upper-bound ripple.